JOURNAL OF CATALYSIS **180,** 14–23 (1998)
ARTICLE NO. CA982262

Surface Properties of Carbided Molybdena–Alumina and Its Activity for CO_2 Hydrogenation

M. Nagai,[1] K. Oshikawa, T. Kurakami, T. Miyao,[2] and S. Omi

Department of Advanced Materials, Graduate School of Bio-Applications and Systems Engineering, Tokyo University of Agriculture and Technology, Koganei, Tokyo 184-8588, Japan

Received July 29, 1997; revised August 19, 1998; accepted August 21, 1998

The surface properties of carbided molybdena–alumina were investigated through O_2-TPD and TPSR along with the catalytic activities of the supported catalysts for CO_2 hydrogenation. The 1173 K-carbided catalyst exhibited the highest activity for the reaction on the CO adsorption basis. H_2 pretreatment of the passivated 973 K-carbided catalyst at 773 K did not affect the activity for CO_2 hydrogenation but a change was visible for the unpassivated catalyst. Through O_2-TPD, it was found that the adsorbed oxygen oxidizes the surface carbon of the molybdenum carbide to form CO_2 and CO. A possible reaction scheme for the hydrogenation of CO_2 is given, along with an explanation for the lowered activity of the passivated catalysts. η-Mo_3C_2 serves as an active site for CO_2 hydrogenation. TPSR results were correlated with the activity to reveal that the number of Mo carbides depends on the activity for CO_2 hydrogenation.

INTRODUCTION

Most catalytic studies of molybdenum carbides have focused on determining the activity of unsupported Mo carbides in such reactions as hydrogenolysis of methylcyclopentane (1) and ethane (2), isomerization of *n*-hexane (3, 4), and hydrogenation of CO and ethylene (2, 5, 6). Although the Mo carbides exhibit high activity, comparable to that of Group VIII metal catalysts, the prepared carbides have confronted several obstacles. First, the carbides are known to have very low surface area values which pose a serious impediment to catalytic application. To overcome this problem industrially, high surface area alumina supports have proven to be effective (3, 7–12). Recent developments in preparation techniques such as the sequential nitridation and carburization of molybdenum oxide to the nitride and carbide resulted in high surface area unsupported carbides (13). A second problem encountered with carburized samples is the accumulation of polymeric carbon onto the support, which causes plugging of the pores and active sites. Hydrotreatment of the carboneous material after carburization effectively removes this carbon contamination to create an active carbide surface. Third, chemisorbed oxygen, surface oxides, and intercalated oxygen atoms act as poisons for most reactions, resulting from the passivation of the carbides with dilute oxygen. Therefore, the catalyst surface should be pretreated to obtain high activity. Treatment prior to reaction has been shown to remove oxygen and carboneous carbon. Four routes of activation, namely the recarburization with hydrogen (3), recarburization with a hydrocarbon (4), addition of a Group VIII metal (3, 4), and addition of K_2CO_3 on molybdenum carbide (14, 15), have been proposed in order to eliminate the surface oxidic layer. Recently, however, Ledoux *et al.* (4) reported that an increase in the specific rate on molybdenum carbide catalyst was obtained through oxidative treatment, resulting in a catalyst which is 25 times more active than platinum catalysts. The oxycarbide has shown greater activity in the isomerization of *n*-hexane (9, 16). It is vital to understand the effects of passivation, or oxygen treatment, which affects the activity of the catalyst. In this study, the effect of passivation on the activity of the carbide catalysts for CO_2 hydrogenation was studied. The effects of H_2 pretreatment and oxidative treatment of carbided Mo/Al_2O_3 were also determined by O_2-TPD. Furthermore, the three carbide species (α-Mo_2C, β-Mo_2C, and η-Mo_3C_2) of molybdenum that are active in the hydrogenation of CO_2 were discussed, based on methane formation through temperature-programmed surface reaction (TPSR).

EXPERIMENTAL

Materials and Catalyst Preparation

Hydrogen and helium (99.9999%) were dried using super Deoxo units (Supelco Co., Oxysorb) and Linde 13X molecular sieve traps prior to use. The 12.5% and 43% MoO_3/Al_2O_3 (Nikki Chemical Co.) were prepared by mixing ammonium paramolybdate with γ-alumina (surface area, 245 m^2g^{-1}). The mixed γ-alumina and ammonium paramolybdate were molded into 3-mm o.d. pellets with a

[1] To whom correspondence should be addressed.

[2] Current address: Department of Applied Chemistry, Kanagawa University, Rokkakubashi, Kanagawa-Ku, Yokohama, 221-8686, Japan.

0021-9517/98 $25.00

kneader, after which the pellets were dried at 393 K for 24 h and calcined at 823 K for 3 h. The 12.5% and 43% MoO_3/Al_2O_3 and 100% MoO_3 were crushed and sieved to 150–250 mesh for characterization and activity measurement. The flow system enabled us to use the reactor as a single-pass differential reactor. All connections and interconnecting lines were assembled in-house, using commercially available stainless steel tubes and Swagelock fittings. The microreactor, used in both the temperature-programmed desorption and the steady-state reaction rate studies, was constructed from a quartz tube (12 mm o.d.), having a total volume of 2.4 ml (17). The catalyst was held in place with a fretted ceramic disk. The microreactor was externally heated, using an oven connected to a variable temperature programmer with a chromel–alumel thermocouple, positioned outside the reactor near the catalyst bed to monitor the temperature and to provide feedback to the PID temperature programmer. A separate thermocouple was placed in the center of the catalyst bed to measure the catalyst temperature. After calcination at 773 K, NH_3 gas (99.999%) was reacted at a flow rate of 4 lh^{-1}, from 573 to 973 K at a rate of 1 $Kmin^{-1}$. After nitriding at 973 K for 3 h, the catalyst was carbided for 3 h at either 773, 973, or 1173 K, using 20% CH_4/H_2 (99.9995%). The samples were passivated using 1% O_2/He for 24 h at room temperature before XRD and elemental analyses. Simplified notations will be used throughout this paper. Molybdenum (MoO_3) loading followed by the nitriding temperature and the carbiding temperature will be abbreviated as follows: 12.5% MoO_3/Al_2O_3 nitrided at 973 K and carbided at 773 K will be referred to as 12N9C7, while 100C9 will denote the unsupported catalyst carbided at 973 K without nitriding.

CO Chemisorption

The quantity of CO chemisorbed on the surface of the carbide catalysts was determined by conventional volumetric analysis (Coulter Co., Omnisorp 100CX). After carburization, the catalysts were cooled to room temperature, taken out of the pretreatment reactor, and transferred to a glove bag without exposure to air. The glove bag was pumped and back-filled with purified helium three times before the catalysts were transferred to a CO experimental quartz cell. Before measuring the CO uptake, the sample was first evacuated at 10^{-2} Pa at 653 K and pretreated in hydrogen (26 kPa) at 653 K for 2 h and 673 K for 1 h. After pretreatment, the catalyst was degassed at 10^{-2} Pa, 673 K for 2 h, then slowly cooled to room temperature in vacuum. The amount of irreversible CO uptake was obtained from the difference between the two isotherms which were extrapolated to zero pressure.

Activity Measurement

The reactivity toward hydrogenation of CO_2 using $CO_2:H_2 = 1:3$ (25 kPa : 75 kPa) was measured *in situ* with the reactor unit under atmospheric pressure after preparation. The reaction was held at 573 K, 101 kPa total pressure. The activity of the 12.5% MoO_3/Al_2O_3 reduced at 673 K for 3 h was also compared. The products formed during the reaction were identified by GC equipped with TCD (Porpak Q, 2m). Qualitative analysis of CO and H_2O was done using a quadrupole mass spectrometer. The reaction rate was calculated by conversion of CO_2 and reported as molecules $min^{-1}g^{-1}$. The turnover frequency (TOF) was expressed as moles of CO_2 converted per moles of irreversible CO adsorbed at room temperature.

O_2-TPD and TPSR

O_2-TPD was carried out *in situ* for the 12.5% and 43% molybdenum loading, the support alone, and for the unsupported catalysts. The catalysts were purged in flowing He (15 $mlmin^{-1}$) for 1 h at 973 K, after which the catalyst was cooled to room temperature. Oxygen (99.999%) was then adsorbed by the pulse method (100 μl), followed by 30 min purging in flowing He. The catalyst was then heated in an He stream at 0.167 K s^{-1} until a final temperature of 1273 K was reached. TPSR was carried out *in situ* for the 12.5% and the unsupported catalysts. The catalysts prepared were purged *in situ* in flowing He (15 $mlmin^{-1}$) after the catalyst was carburized. Helium was switched to H_2 (99.9995%) and the catalyst was heated in flowing H_2 (15 $mlmin^{-1}$) at a rate of 10 $Kmin^{-1}$ from 373 to 1273 K. The gases released during O_2-TPD and TPSR were analyzed with a quadrupole mass spectrometer (ULVAC, MSQ-150A) equipped with a variable-leak valve maintained at about 350 K through the use of heating tape. The desorption rates of CO_2 ($m/z = 44$), CH_4 ($m/z = 16$), and NH_3 ($m/z = 15$) gases and water ($m/z = 18$) were calculated through calibration curves for each gas. The spectra of the gases were fitted using a nonlinear squares method with a Gaussian–Lorentzian function after an FFT filter smoothing of the spectra.

X-Ray Diffraction Pattern

XRD spectra before and after O_2-adsorption TPD were taken for the powdered unsupported catalyst with a RAD II, Rigaku Electronics Co., using a CuK_α ray at 30 kV, 20 mA. The crystallite size of the catalyst was estimated from the broadening of the more intense diffraction lines of phase fcc α-Mo_2C (200) using the Scherrer equation. The peaks in the spectra were identified using ASTM cards.

RESULTS AND DISCUSSION

Catalytic Activity of Carbided 12.5% Mo/Al_2O_3 Catalyst for CO_2 Hydrogenation

The main products formed were CO and H_2O, suggesting the occurrence of the reverse water gas shift reaction,

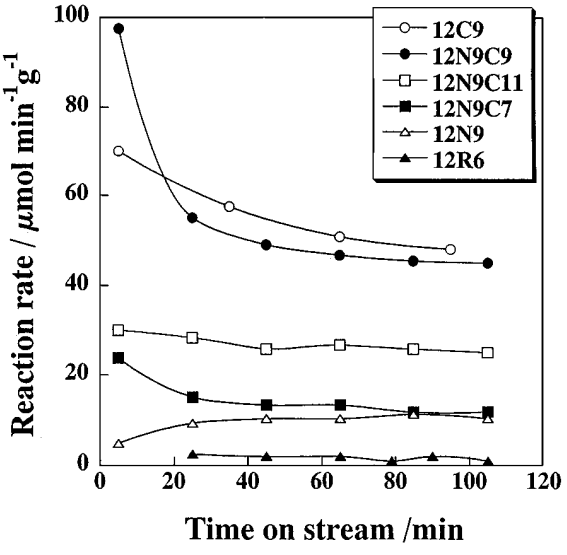

FIG. 1. Variation of CO_2 reduction rate at 573 K with time on stream. ○, 12C9; ●, 12N9C9; □, 12N9C11; ■, 12N9C7; △, 12N9; and ▲, 12R6.

$CO_2 + H_2 \rightarrow 2CO + H_2O$. The formation of other hydrocarbon compounds such as CH_4 (18) and methanol (19) could not be confirmed for the carburized 12.5% Mo/Al_2O_3, since the reaction was held at atmospheric pressure. The rates of CO_2 hydrogenation for the 12.5% Mo/Al_2O_3 carbided at three temperatures are shown in Fig. 1. The rates of CO_2 hydrogenation for the 673 K-reduced and 973 K-nitrided catalysts are also shown for comparison. A maximum reaction rate was observed for the carburization temperature of 973 K, as portrayed by the reaction rate values for 12C9 and 12N9C9, while 12N9C11 maintained constant activity. It was also observed that the deactivation rate for the 12N9C9 catalyst was faster than 12N9C11 and the other 973 K-carbided catalysts. The catalysts without carburization treatment, 12N9 and 12R6, had low activity.

CO irreversible uptake for the 12N9C11 sample amounted to 2.5 $\mu molg^{-1}$, which was the smallest value of all the catalysts, as shown in Table 1. Using these values to calculate the TOF values for the hydrogenation of CO_2,

TABLE 1

CO Uptake and Catalytic Activities of Carbided Samples

Catalyst	Total CO ($\mu molg^{-1}$)	Irreversible CO ($\mu molg^{-1}$)	Reaction rate ($\mu mols^{-1}g^{-1}$)	TOF ($molg^{-1}s^{-1}$/ $COmolg^{-1}$)
12N9C11	12.5	2.5	0.433	0.173
12N9C9	51.7	11.4	0.778	0.0683
12C9	37.6	9.3	0.847	0.0910
12N9C7	41.7	14.3	0.220	0.0154
12N9	67.0	25.0	0.170	0.0068
12R6	22.6	5.5	0.0325	0.0054

TABLE 2

Catalytic Activity of Alumina-Supported Molybdenum Carbides at 573 K

	Rate ($\mu mols^{-1}g\text{-}cat^{-1}$)			
	Unpassivated		Passivated	
Catalyst carbided at 973 K	Without pretreatment	H_2 pretreatment at 773 K	Without pretreatment	H_2 pretreatment at 773 K
12N9C9	0.733	0.778	0.683[a]	0.692(0.490)[c]
12C9	0.847	0.907	0.647[a,d]	0.650[b](0.465)[c]

[a] After carburization at 973 K, the catalyst was passivated in flowing 1% O_2/He at room temperature and subsequently used for the activity measurement.

[b] The catalyst was passivated at room temperature with 1% O_2/He after carburization and then reduced at 773 K in flowing 25 $mlmin^{-1}$ H_2.

[c] The catalyst was first reduced at 773 K in flowing 25 $mlmin^{-1}$ H_2 and subsequently passivated with 1% O_2/He at room temperature.

[d] Irreversible CO uptake is 17.4 $\mu mlog^{-1}$, resulting to the TOF of 0.0372 s^{-1}.

the 12N9C11 sample exhibited the highest value per CO chemisorption site. The 973 K-carbided catalyst are also active in CO_2 hydrogenation. Although the 12N9C7 and 12N9 samples exhibited high CO uptake, the CO_2 hydrogenation rate was low, resulting in a low TOF value.

The Effect of Passivation of Supported Carbides on the Catalytic Activity

The rates of CO_2 hydrogenation for the unpassivated and passivated 12.5% Mo/Al_2O_3 catalysts carbided at 973 K are shown in Table 2. The passivated molybdenum carbide catalysts were less active than the unpassivated catalysts for CO_2 hydrogenation. The H_2 pretreatment of the passivated 12N9C9 and 12C9 catalysts at 773 K had little effect on the activity for CO_2 hydrogenation but a change was visible for the activity of the unpassivated catalysts. The unpassivated 12C9 catalyst reduced at 773 K in H_2 showed the highest rate. Since the passivation lowered the activity of 12C9 more than that of 12N9C9, it is deduced that nitridation produced nitrogen–carbon bonds (C/Mo = 0.37 and N/Mo = 0.33 in Table 3) which protect the decomposition of carbides or carbo-nitrides with the O_2 atoms inserted into the carbide bulk. H_2 treatment at 773 K before passivation (9, 20) exposed the active sites, but passivation covered the catalyst surface with O_2, resulting in lowered catalytic activity for CO_2 hydrogenation. Leary *et al.* (6) reported that O_2 covered the vacancy sites more strongly than the carbide sites. In this study, the H_2 treatment of the passivated catalysts at 773 K removed the carbon of molybdenum carbide to expose active sites on the surface. It was concluded that the passivation lowered the activity of carbided molybdenum–alumina for CO_2 hydrogenation.

TABLE 3

Surface Area and Carbon Content of Carbided Samples

Catalyst	Specific surface area (m^2g^{-1})	C[a]/Mo[b]		N[a]/Mo[b]
		Before TPSR	After TPSR	Before TPSR
100N9C11	—[d]	4.52	5.10	0.01
100N9C9	88	0.49	0.44	0.03
100C9	7	0.52	0.49	0
100N9C7	—[d]	0.02	0.02	0.50
100Fresh[c]	1	0	0	0
12N9C11	198	9.11	8.66	0.09
12N9C9	230	0.37	0.10	0.33
12C9	213	0.48	0.13	0
12N9C7	197	0.10	0.08	0.54

[a] Determined by elemental analysis.
[b] Determined by atomic absorption spectroscopy.
[c] Fresh unsupported-oxide before nitriding on carburization.
[d] Not determined.

O_2-TPD and Changes in XRD Spectra before and after O_2-TPD

O_2-TPD experiments were carried out to study the effects of oxidative treatment on molybdenum carbide and polymeric carbon of the carbided catalysts. The changes in the desorption spectra of CO_2 and CO for TPD of the O_2 adsorbed on the samples are shown as a function of molybdenum loading in Fig. 2. The desorption species detected during O_2-TPD were CO and CO_2. It should be stressed that H_2O and O_2 were not observed for the temperature ranges selected in this experiment. For alumina without molybdenum, the desorption of CO_2 was not observed. For the 12N9C9 sample, small peaks of CO_2 desorption were observed at 700 K with a shoulder peak at 540 K, and the two peaks at 450 and 620 K increased with molybdenum loading for the Mo/Al_2O_3 catalyst. The unsupported sample, 100N9C9, showed three distinct desorption peaks at 450, 620, and 1100 K. For 100C9, a large peak at 850 K together with a peak increasing above 1100 K was observed. From the CO_2 desorption peak of 100N9C9, it was calculated that the CO_2 desorption peak amounted to 76% of the surface molybdenum carbide. In Fig. 2B, the peaks for CO desorption were observed at higher temperatures than those of CO_2 desorption. The 100N9C9 differed from the supported sample in that the CO desorption was observed at 780 K, with the 1100-K peak being notably distinct. The samples carburized at 1173 K (12N9C11 and 100N9C11) were covered with a large amount of carbon, as shown in Table 3. O_2 adsorption TPD was carried out for 12N9C11 with polymeric carbon on the surface to determine the effects of oxygen for the desorption of polymeric carbon. The results are shown in Fig. 3, revealing a small amount of CO desorption. The presence of polymeric carbon on the surface of 12N9C11 showed CO desorption above 760 K in the TPD profile without CO_2 desorption.

The XRD spectra before and after TPD of O_2 adsorbed on the unsupported Mo carbide are given in Fig. 4. For 100N9C9, structural changes from fcc α-Mo_2C to hcp β-Mo_2C were observed along with the formation of Mo metal. The 100C9 exhibited hcp β-Mo_2C, while the 100N9C11 sample consisted of η-Mo_3C_2. Although the sample was exposed in air, the XRD measurement did not detect the oxidic form of MoO_2 and MoO_3.

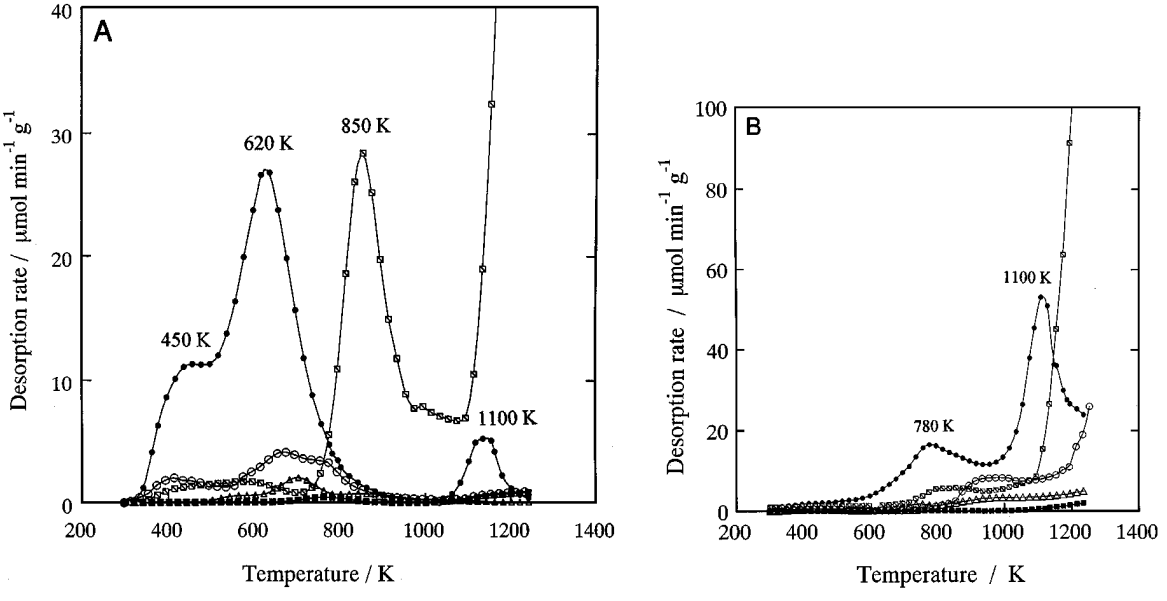

FIG. 2. Changes in the desorption spectra of (A) CO_2 and (B) CO for O_2 adsorption TPD of the molybdenum carbides as a function of Mo loading. ●, 100N9C9; □, 100C9; ○, 43N9C9; △, 12N9C9; ■, 0N9C9.

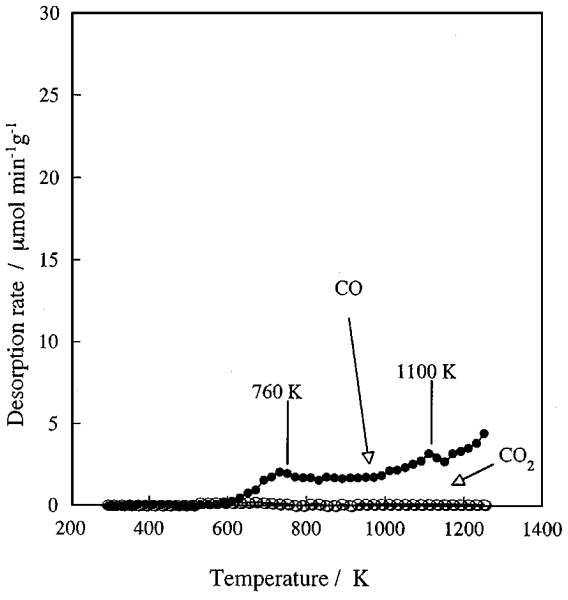

FIG. 3. CO and CO_2 desorption during O_2 adsorption TPD over supported molybdenum carbide (12N9C11).

In Fig. 5a, O_2-TPD was carried out up to 800 K, the temperature at which the CO_2 peaks appearing in the lower temperature regions desorb. The catalyst was then cooled in He to room temperature, after which the O_2-TPD experiment was repeated, this time to the final temperature of 1139 K (Fig. 5b). As the XRD results revealed the transformation of fcc α-Mo_2C into hcp β-Mo_2C and Mo metal during the temperature range of O_2-TPD, a hypothesis was established that the CO_2 desorption peaks correspond with the phase transformation of the carbide. From the results, the peaks of CO_2 desorption at 842 and 634 K were ascribed to CO_2 desorption from reaction of O_2 with β-Mo_2C and α-Mo_2C, respectively. The desorption peaks of CO_2 at 620 and 1100 K for 100N9C9 in Fig. 2A are due to the transformation of fcc α-Mo_2C into hcp β-Mo_2C and the partial reduction of β-Mo_2C to Mo metal, respectively. The fcc α-Mo_2C structure changed to the thermodynamically more stable hcp β-Mo_2C. The particle size of the crystallite (fcc α-Mo_2C) before O_2-TPD was determined from the Scherrer equation to be 9.8 nm, whereas this value increased to 32.0 nm after O_2-TPD. The peak at 450 K was probably

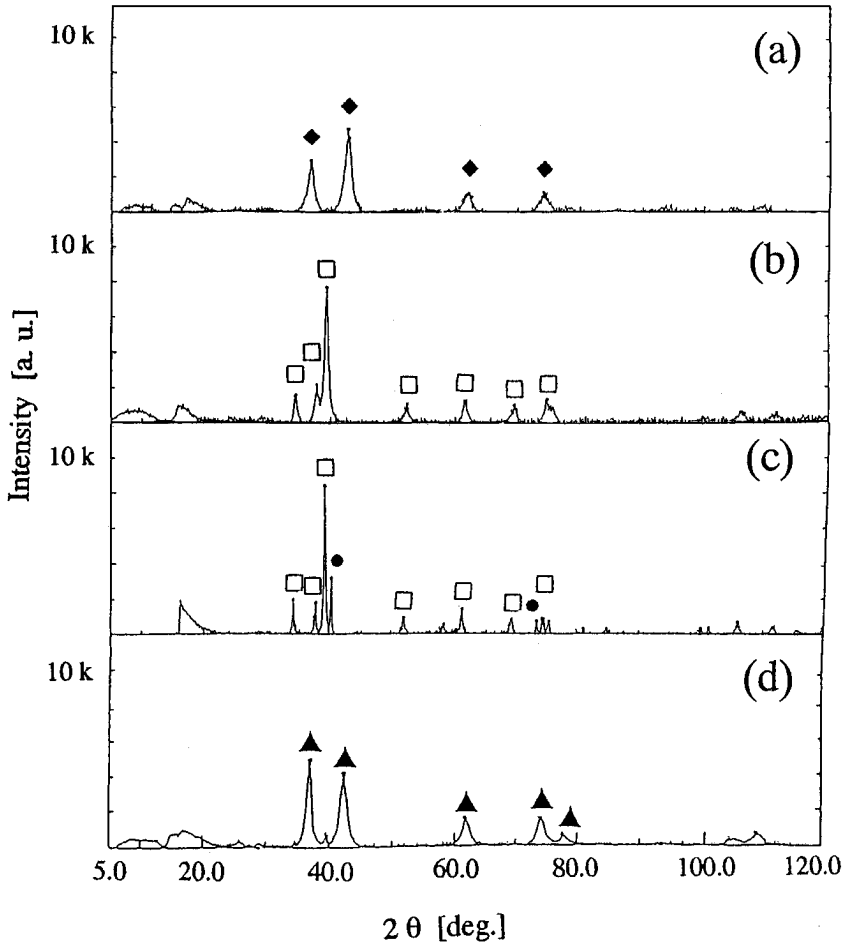

FIG. 4. The XRD spectra before and after O_2 adsorption TPD of the unsupported Mo carbide. (a) 100N9C9; ◆, α-Mo_2C (fcc); (b) 100C9; □, β-Mo_2C (hcp); (c) 100N9C9 after O_2 TPD; □, β-Mo_2C (hcp); ●, Mo metal; (d) 100N9C11; ▲, η-Mo_3C_2.

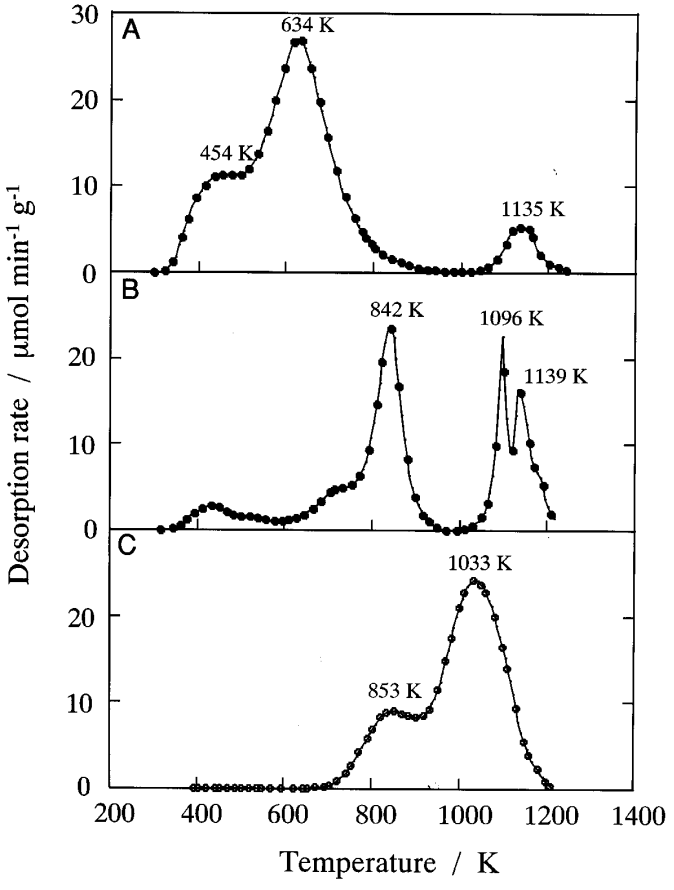

FIG. 5. CO_2 desorption in (A) O_2-TPD and the subsequent (B) O_2-TPD, and (C) TPSR for 100N9C9.

due to CO_2 adsorption. Since molybdenum oxides were not detected in the O_2-exposed catalyst before and after O_2-TPD up to 1270 K, the oxygen is thought to adsorb on the crystalline carbide instead of the molybdenum metal. The adsorbed O_2 then extracted carbon in molybdenum carbide during TPD to form CO or CO_2, ultimately leading to the reduction of the molybdenum carbide to form molybdenum metal. Furthermore, the amount of carbon calculated from CO and CO_2 formed during O_2-TPD was 1.97 mmol/g, 40.2% of total carbon of 100N9C9. This value was large compared to the carbon content (22%) calculated during TPSR, as mentioned later. In light of the fact that a large amount of oxygen enters the crystal structure of the bulk (6, 21, 22) and the interatomic distance within the Mo_2C structure, 0.3 nm, is not large enough to accommodate dioxygen, it is most likely that the O_2 dissociates on the catalyst surface, diffusing into the crystal structure as atomic oxygen.

The formation of CO and CO_2 during the O_2-TPD may be explained as follows: first the oxygen adsorbs dissociatively and then it bonds to the carbidic carbon. As more heat is applied, desorption in the form of CO occurs, leading to the formation of metal Mo species, which is supported by the results from XRD. The reaction of this CO with the surface oxygen species causes the formation of CO_2. Thus, the presence of excess oxygen species on the catalyst surface induces the formation of CO_2, which may explain the decreased activity of the passivated catalyst.

Surface Species through TPSR

To correlate the activity of the catalysts for CO_2 hydrogenation with carbon and carbides on the surface of the carbided catalysts, TPSR experiments were carried out for the catalysts pretreated in those conditions. The type of carbides on the surface of the carbided catalysts has been identified by the temperature of CH_4 evolution during TPSR. TPSR profiles of the molybdenum carbide catalysts are shown in Fig. 6A. The main gaseous products obtained by TPSR were CH_4 and N_2, while other carbon-containing gases such as CO or CO_2 were not detected. The TPSR technique was used previously by Lee *et al.* (23, 24) to distinguish between surface carbide, pyrolytic carbon, and graphitic carbon in unsupported molybdenum carbide. Pyrolytic carbon is a pregraphitic form of reactive carbon obtained by thermal cracking of hydrocarbon gases. From the XRD study, the presence of three distinct carbon species

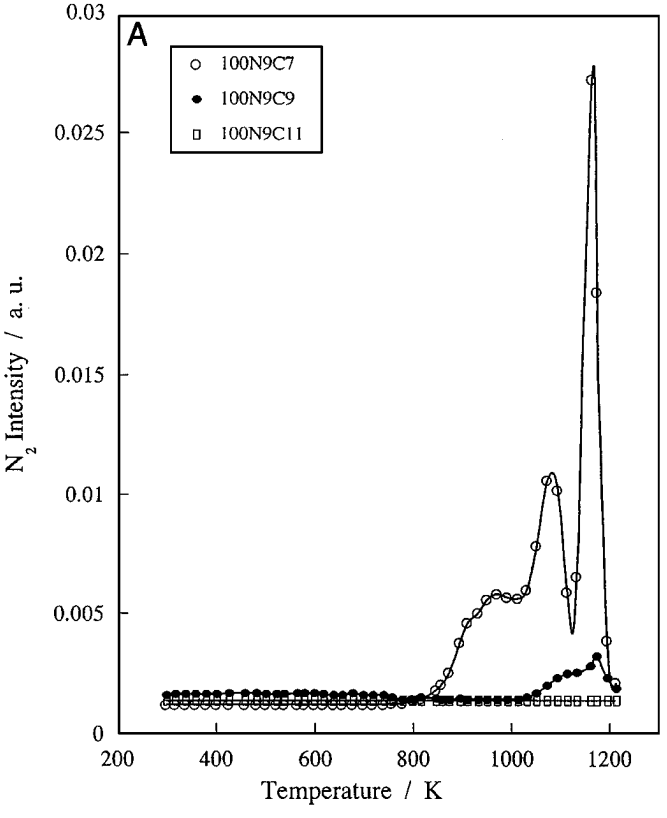

FIG. 6A. The N_2 desorption in TPSR profiles for molybdenum carbide catalyst. ○, 100N9C7; ●, 100N9C9; and □, 100N9C11.

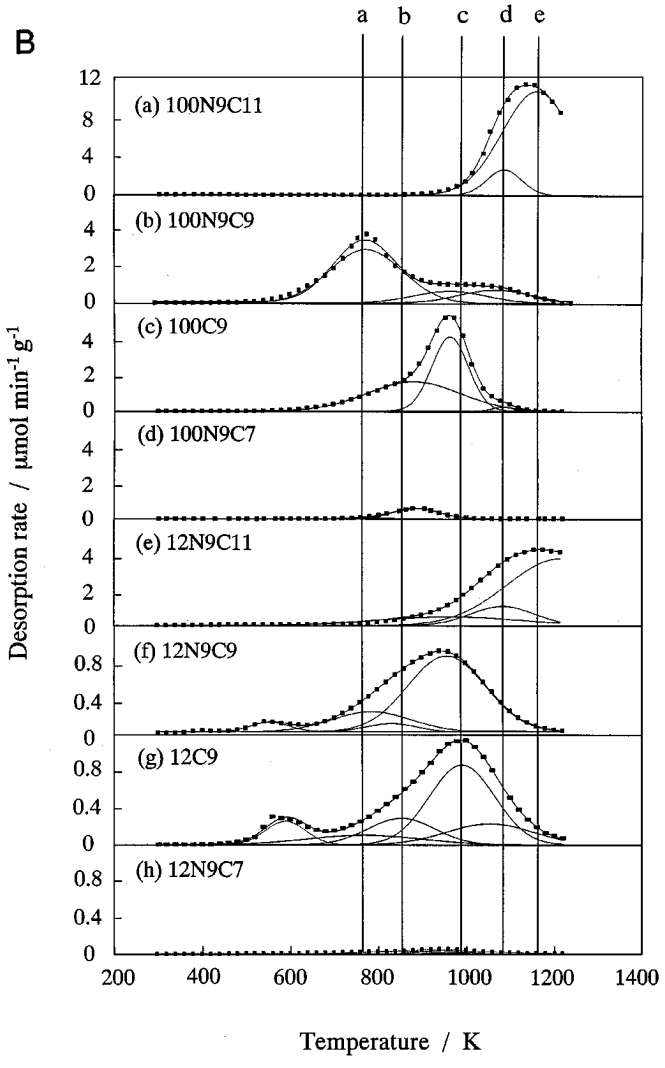

FIG. 6B. The CH_4 desorption in TPSR profiles over molybdenum carbide catalysts.

on the surface molybdenum carbides, α, β, and η, was observed. Correlating this data to the TPSR results shown in Fig. 6B, the b peak was attributed to β-Mo_2C for 100C9, while the peaks d and e are due to η-Mo_3C_2 and graphitic carbon from 100N9C11, respectively. The CH_4 desorption peaks in the TPSR spectra of the molybdenum carbide catalysts were deconvoluted into five peaks, as shown in Fig. 6B. The amount of CH_4 evolved from TPSR for each carbided catalyst is shown in Table 4. For the 12N9C7 and 100N9C7 catalysts, the methane peak was small, while the desorption of N_2 gas was observed at 1053 K for 100N9C7 (Fig. 6A) and 12N9C7 (23, 24). It was found that the carbon uptake of the catalysts (100N9C7 and 12N9C7) was small, while the nitrogen content remained stoichiometric (N/Mo = 0.5 in Table 3). From the result, carbide and polymeric carbon were scarcely formed in the carburization at 573 K. In light of the fact that the N_2 desorption profile (12N9C7) was similar to that of the Mo nitride, 12N9 (25, 26), it can be deduced that the molybdenum nitride was not transformed into molybdenum carbide below 773 K. In Fig. 6B, a broad peak of methane for the 12N9C9 catalyst was seen at 943 K, deconvoluted into the peaks, a, b, c, and d. The carbidic carbon d peak for the supported sample 12C9, especially 12N9C11 was greater than that for the 12N9C9. The C/Mo ratio increased from 0.37 (12N9C9) to 0.48 (12C9). Furthermore, the surface area for 12C9 was 10% less than that for 12N9C9. Prenitriding of the unsupported catalyst before carburization results in a tenfold increase in surface area.

For 12N9C11, the TPSR spectra showed no peaks of a and b of molybdenum carbides but was deconvoluted into c, d, and e. With a maximum at 1213 K the high temperature peak, e, observed with the sample carburized at 1173 K is due to graphitic carbon. O_2-TPD followed by TPSR (Fig. 5c) showed that the peaks at 853 and 1033 K in the TPSR spectra increased as the peak at around 770 K decreased. Since α-Mo_2C was transformed to β-Mo_2C during the first O_2-TPD, peak b was ascribed to CH_4 formed from β-Mo_2C. As mentioned previously, the carbon content in 100N9C11 was high, although XRD showed η-Mo_3C_2. Consequently, the peaks d and e in TPSR are due to the release of CH_4 from η-Mo_3C_2 and graphite carbon. Therefore, the a, b, and d peaks of methane desorption for the supported catalysts at about 770, 850, and 1050 K were attributed to the desorption of methane during the decomposition of carbidic carbons, i.e., α-Mo_2C, β-Mo_2C, and η-Mo_3C_2,

TABLE 4

Deconvoluted CH_4 Desorption from TPSR of Various Molybdenum Carbides

Catalyst	Desorption of CH_4 deconvoluted (μmolg^{-1}) [peak temp./K] a	b	c	d	e	Total desorption of CH_4 (μmolg^{-1})
100N9C11	—	—	—	123 [1085]	781 [1159]	905
100N9C9	315 [779]	—	27 [946]	84 [1056]	—	426
100C9	—	217 [881]	218 [963]	7 [1083]	—	442
100N9C7	—	—	—	—	—	—
12N9C11	—	—	9.3 [963]	93 [1083]	282 [1213]	468
12N9C9	22 [773]	6 [844]	80 [953]	1 [1015]	—	109
12C9	14 [767]	23 [852]	68 [959]	23 [1052]	—	128
12N9C7	—	2 [847]	1.5 [942]	2 [1052]	—	5.5

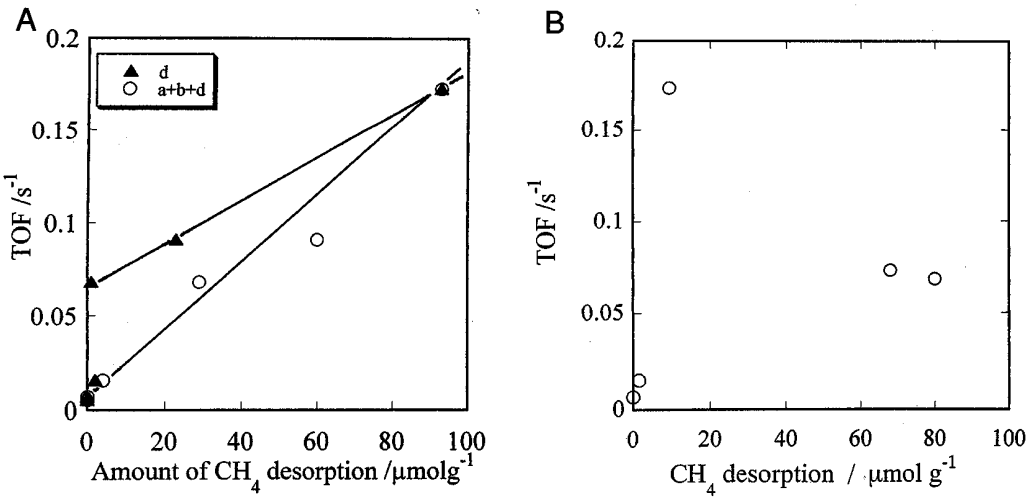

FIG. 7. The TOF in CO_2 hydrogenation as a function of (A) CH_4 desorption from (▲) d and (○) (a + b + d) carbides, in TPSR of 12N9N11, 12N9C9, 12C9, and 12N9C7, and (B) CH_4 desorption of c carbon.

respectively. The c and e peaks at about 960 and 1210 K were assigned to surface pyrolytic carbon and graphitic carbon, respectively.

Surface Carbide and Its Activity for CO_2 Hydrogenation

The varying activities of 12.5% Mo/Al_2O_3 catalysts for CO_2 hydrogenation can be explained by the presence of the different carbide and carbon species, as outlined above. The TOF as a function of the desorption of CH_4 for each of the carbidic species (a, b, and d) and the carbon species (c) is given in Fig. 7. The graphite species (e), only in 12N9C11, could not be estimated for the activity relationship for the e peak. There is a good relationship between the TOF and the CH_4 desorption peaks of d and (a + b + d) carbides. The linear relationship shows that molybdenum carbides are active sites for CO_2 hydrogenation (Fig. 7A). The lack of activity for the c peak, designated as pyrolytic carbon, shows how graphite acts as a poison for this reaction. Thus, the differences in the activities shown in Fig. 7 is explained as follows. Although 12N9C11 contained much graphitic carbon, η-Mo_3C_2 in 12N9C11 is more active than α-Mo_2C and β-Mo_2C. A decrease in η-Mo_3C_2 (d) lowers the activities (12N9C9 and 12C9) in Fig. 7A. The lack of the carbidic species diminishes the activity, as can be seen for 12N9C7, although the contribution of molybdenum nitride cannot be ignored. Thus, the molybdenum carbides, especially η-Mo_3C_2, are the active species for CO_2 hydrogenation.

The reaction scheme for CO_2 hydrogenation on the molybdenum carbide catalyst is shown in Fig. 8. The CO_2 adsorbs onto the coordinated unsaturated site of molybdenum carbide, which leads to the dissociation of CO_2. As this process proceeds, hydrogen reacts with the dissociative oxygen from CO_2, forming water. The desorption of both species completes the cycle, leaving a coordinated unsaturated site available for another CO_2 hydrogenation to take place. When CO_2 adsorbs dissociatively on molybdenum

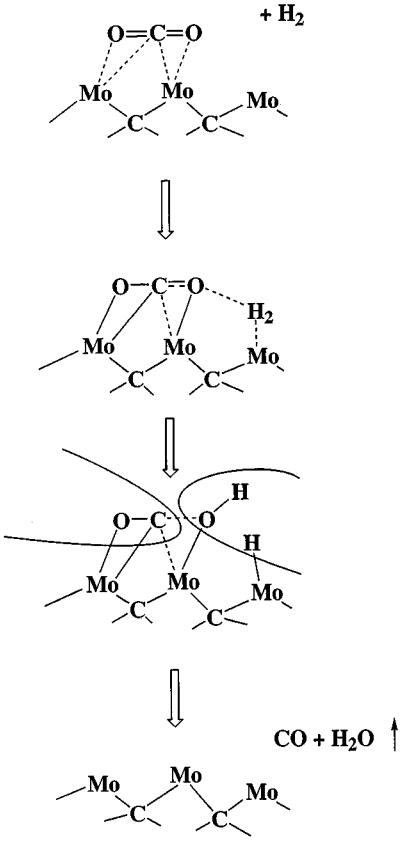

FIG. 8. Model depicting hydrogenation of CO_2 on molybdenum carbide.

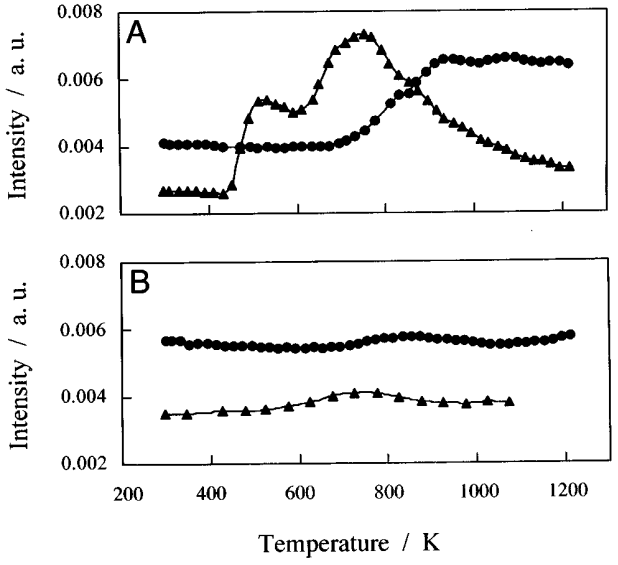

FIG. 9. The H_2O desorption in (▲) TPD and (●) TPSR over 12N9C9 catalyst (B) before and (A) after CO_2 hydrogenation 10 h on stream at 573 K.

carbide, atomic oxygen migrates into the bulk and the dissociative CO is desorbed during TPD.

Surface Oxygen Species after Reaction

The TPD in He and the subsequent TPSR in H_2 was carried out without exposing the spent 12N9C9 catalysts to air, in order to better understand the nature of the residual oxygen species of the carbide catalyst after 10 h on stream at 573 K. The TPD and TPSR of the spent 12N9C9 revealed the following results (Fig. 9A). The peaks observed for H_2O desorption were 573 and 773 K during TPD, while the formation of H_2O was observed above 773 K during TPSR after TPD. Since 12N9C9 involved the formation of CO and H_2O during the reaction, the formation of water at two desorption temperatures during the first TPD of the spent catalyst was due to physically adsorbed water and to a product of a reverse water gas shift reaction of the adsorbed species. In Fig. 9B, no formation of water was observed in flowing He in TPD and H_2 in TPSR, suggesting that the 12N9C9 was fully carbided at 973 K. The result reveals that oxygen remains within the carbide structure as well as with the water formed during CO_2 hydrogenation. Since the water forms above 773 K during the second TPSR of the spent catalyst, it can be deduced that this water is not a product of a reverse water gas shift reaction of the adsorbed water species, but rather the product of the reduction of surface Mo oxides formed during the reaction. Thus, the catalytic activity toward CO_2 hydrogenation decreases with the formation of surface Mo oxides during the reaction of oxygen treatment of the supported molybdenum carbide catalyst.

CONCLUSIONS

(1) The 12N9C11 catalyst carbided at 1173 K exhibits greater values for the reaction rate than the 773 K- and 973 K-carbided samples. The 100N9C11 consisted of η-Mo_3C_2. The catalytic activity towards CO_2 hydrogenation decreases with oxygen treatment of the supported molybdenum carbide catalyst.

(2) The CH_4 desorption peaks in the TPSR spectra can be deconvoluted into 5 peaks, as shown in Fig. 6B, suggesting the presence of three carbide and two carbon species on the surface. The peaks at about 770, 850, and 1050 K are attributed to decomposition of carbidic carbons, i.e., α-Mo_2C, β-Mo_2C, and η-Mo_3C_2, respectively. The peaks at about 960 and 1210 K are most likely due to the decomposition of pyrolytic and graphitic carbons. The linear relationship between the methane desorption for the molybdenum carbides and the TOF values for CO_2 hydrogenation shows that a carbidic carbon is indeed an active site for this reaction.

(3) Adsorbed oxygen oxidizes the surface carbon of the molybdenum carbide to form CO_2 from 400 to 1000 K. The transformation of fcc α-Mo_2C into hcp β-Mo_2C and Mo metal occurs during the temperature range of O_2-TPD. The desorption peaks of CO_2 at 620 and 1100 K for 100N9C9 are due to the transformation of fcc α-Mo_2C into hcp β-Mo_2C and the partial reduction of β-Mo_2C to Mo metal, respectively.

ACKNOWLEDGMENT

The authors acknowledge partial financial support extended from a Grant-in-Aid for Scientific Research of the Ministry of Education of the Japanese Government under Contract (07044132).

REFERENCES

1. Sato, Y., Imai, D., Sato, A., Kasahara, S., Omata, K., and Yamada, M., *J. Jpn. Petro. Inst.* **37**, 514 (1994).
2. Ranhotra, G. S., Bell, A. T., and Reimer, J. A., *J. Catal.* **108**, 40 (1987).
3. Ledoux, M. J., Huu, C. P., Guille, J., and Dunlop, H., *J. Catal.* **134**, 383 (1992).
4. Ledoux, M. J., Pham-Huu, C., Dunlop, H., and Guille, J., *in* "Proceedings, 10th International Congress on Catalysis, Budapest, 1992" (L. Guczi, F. Solymosi, and P. Terenyi, Eds.), p. 955. Akadémiai Kiadó, Budapest, 1993.
5. Saito, M., and Anderson, R. B., *J. Catal.* **63**, 483 (1980).
6. Leary, K. J., Michaels, J. N., and Stacy, A. M., *J. Catal.* **101**, 301 (1986).
7. Lee, J. S., Yeom, M. H., Park, K. Y., Nam, I.-S., Chung, J. S., Kim, Y. G., and Moon, S. H., *J. Catal.* **128**, 126 (1991).
8. Lee, J. S., Lee, K. H., and Lee, J. Y., *J. Phys. Chem.* **96**, 362 (1992).
9. Pham-Huu, C., Ledoux, M. J., and Guille, J., *J. Catal.* **143**, 249 (1993).
10. Boudart, M., Oyama, S. T., and Leclercq, L., *in* "Proceedings, 7th International Congress on Catalysis, Tokyo, 1980" (T. Seiyama and K. Tanabe, Eds.), p. 578. Elsevier, Amsterdam, 1981.
11. Sajkowski, D. J., and Oyama, S. T., *Appl. Catal.* **134**, 339 (1996).
12. Aegerter, P. A., Quigley, W. W. C., Simpson, G. J., Ziegler, D. D., Logan, J. W., McCrea, K. R., Glazier, S., and Bussell, M. E., *J. Catal.* **164**, 109 (1997).

13. Volpe, L., and Boudart, M., *J. Solid State Chem*. **59**, 348 (1985).
14. Park, K. Y., Seo, W. K., and Lee, J. S., *Catal. Lett.* **11**, 349 (1991).
15. Woo, H. C., Park, K. Y., Kim, Y. G., Nam, I.-S., Chung, J. S., and Lee, J. S., *Appl. Catal.* **75**, 267 (1991).
16. Delporte, P., Meunier, F., Pham-Huu, C., Vennegues, P., Ledoux, M. J., and Guille, J., *Catal. Today* **23**, 251 (1995).
17. Nagai, M., Koizumi, K., and Omi, S., *J. Jpn. Petro. Inst.* **39**, 272 (1997).
18. For the unsupported catalyst carburized at 993 K (100C9/100N9C9), methane was formed with 33% selectivity to CO at 573 K and atmospheric pressure.
19. Dubois, J.-L., Sayama, K., and Arakawa, H., *Chem. Lett.* 5 (1992). The reaction conditions were 6 MPa of total pressure ($Ar/H_2/CO_2 = 10.1/22.7/67.2$).
20. Miyao, T., Shishikura, I., Matsuoka, M., Nagai, M., and Oyama, S. T., *Appl. Catal. A* **165**, 419 (1997).
21. Ranhotra, G. S., Haddix, G. W., Bell, A. T., and Reimer, J. A., *J. Catal.* **108**, 24 (1987).
22. Ribeiro, F. H., Dalla Betta, R. A., Guskey, G. J., and Boudart, M., *Chem. Mater.* **3**, 805 (1991).
23. Lee, J. S., Volpe, L., Ribeiro, F. H., and Boudart, M., *J. Catal.* **112**, 44 (1988).
24. Lee, J. S., Oyama, S. T., and Boudart, M., *J. Catal.* **106**, 125 (1987).
25. Nagai, M., Miyata, A., Kusagaya, T., and Omi, S., *in* "The Chemistry of Transition Metal Carbides and Nitrides" (S. T. Oyama, Ed.), p. 327. Blackie, London, 1996.
26. Nagai, M., Kusagaya, T., and Omi, S., *Bull. Soc. Chim. Belg.* **104**, 311 (1995).